

# An Efficient Algorithm for Multiphase Image Segmentation with Intensity Bias Correction

Haili Zhang, Xiaojing Ye, and Yunmei Chen

**Abstract**—This paper presents a variational model for simultaneous multiphase segmentation and intensity bias estimation for images corrupted by strong noise and intensity inhomogeneity. Since the pixel intensities are not reliable samples for region statistics due to the presence of noise and intensity bias, we use local information based on the joint density within image patches to perform image partition. Hence, the pixel intensity has a multiplicative distribution structure. Then, the maximum-a-posteriori (MAP) principle with those pixel density functions generates the model. To tackle the computational problem of the resultant nonsmooth nonconvex minimization, we relax the constraint on the characteristic functions of partition regions, and apply primal-dual alternating gradient projections to construct a very efficient numerical algorithm. We show that all the variables have closed-form solutions in each iteration, and the computation complexity is very low. In particular, the algorithm involves only regular convolutions and pointwise projections onto the unit ball and canonical simplex. Numerical tests on a variety of images demonstrate that the proposed algorithm is robust, stable, and attains significant improvements on accuracy and efficiency over the state-of-the-arts.

**Index Terms**—Image segmentation, intensity inhomogeneity, optimization methods, minimax techniques.

## I. INTRODUCTION

IMAGE segmentation has been an active research area in computational vision and pattern analysis with a wide range of applications. In particular, the emerging developments in medical imaging demand effective and robust algorithms for image segmentation, such as organ or tumor detection and tissue classification. Approaches to image segmentation can be roughly classified into two categories: edge-based models (e.g. [1]–[5]) and region-based models (e.g. [6]–[11]). Edge-based models rely on edge information to locate the boundaries of regions. Region based models partition the image domain into several disjoint regions such that each region exhibits distinct statistical properties from those by others. It is also noted that most of these methods explicitly or implicitly assume intensity homogeneity of input images. However, in many real world applications, images encounter

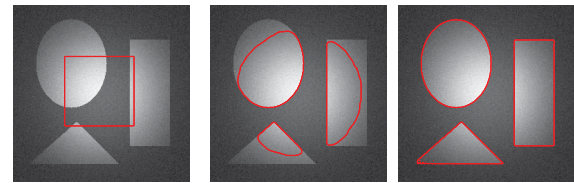


Fig. 1. Image segmentation in the presence of intensity bias. Left: input image with a square initial partition contour in red. Middle: result of segmentation assuming piecewise constant intensity. Right: result of segmentation with bias correction.

significant intensity inhomogeneity due to spatial variations in illuminations and physical constraints in acquisition sensitivities. For example, in magnetic resonance (MR) imaging, intensity inhomogeneity is presented as bias field mainly caused by nonuniform magnetic fields [12]. In these cases, the same object in a given image may exhibit various contrasts at different locations of the image domain. These large variations in image intensities can cause false identification of regions as a consequence of ambiguous statistics presented by pixel intensities. For instance, the widely used Chan-Vese model which assumes piecewise constant intensity in each region cannot generate correct segmentation due to intensity inhomogeneity as shown in the middle of Figure 1. On the other hand, a desired segmentation can be obtained by taking the intensity inhomogeneity into account, as shown on the right of Figure 1. Therefore, segmentation for images with inhomogeneous intensities is a challenging problem, and usually requires a combination of segmentation and intensity bias correction.

There have been a series of work proposed to tackle the segmentation problem with intensity biases in images (e.g. [12]–[21] and references therein). Due to the space limitation, we here only review several very recent models that are closely related to the present work. In [20], the authors proposed a variational model for tissue classification of MR images. In their model, local intensities of different tissues within a neighborhood were used to form separable clusters, where the centers are approximated by the product of the bias within the neighborhood and a tissue-dependent constant. This local clustering criterion is combined with membership functions to form an energy functional. Then the tissue classification and bias field estimation are simultaneously achieved by estimating the membership functions, bias field, and the parameters that approximate the true signals in each region via minimizing the energy functional. In [22], a minimization framework was developed for multiphase segmentation and bias correction.

Manuscript received February 6, 2012; revised February 3, 2013; accepted April 20, 2013. Date of publication May 13, 2013; date of current version August 28, 2013. The associate editor coordinating the review of this manuscript and approving it for publication was Prof. Jeffrey A. Fessler.

H. Zhang and Y. Chen are with the Department of Mathematics, University of Florida, Gainesville, FL 32611 USA (e-mail: hlzhang@ufl.edu; yun@ufl.edu).

X. Ye is with the School of Mathematics, Georgia Institute of Technology, Atlanta, GA 30332 USA (e-mail: xye33@math.gatech.edu).

Color versions of one or more of the figures in this paper are available online at <http://ieeexplore.ieee.org>.

Digital Object Identifier 10.1109/TIP.2013.2262291

This model used the same local clustering criterion as that in [20] to define an energy functional in level set formulation. Later, Li *et al.* extended their model in [21] to simultaneous multi-phase segmentation and bias correction. In [21], multiple level set functions were used to represent the subregions. Minimization of the energy was achieved by an interleaved process of level set evolution [23] and the estimation of the bias field. Recently, Zhang *et al.* in [24] also proposed a level set approach for simultaneous tissue segmentation and bias correction for MR images. But different from the work in [20]–[22], where the intensities in each cluster were approximated by its mean in  $L^2$  sense, in their model local intensities of different tissues were assumed to be distributed as Gaussians with the means as the centers of the cluster and variances to be optimized.

The aim of this paper is to build a joint image segmentation and bias field correction framework that unifies these recent models, and to develop an efficient numerical algorithm to solve the model efficiently. We consider a multiplicative structure of intensity density function for center points of image patches, then we utilize the maximum-a-posteriori (MAP) principle to construct a generalized model for joint image segmentation and bias field estimation. Besides the modeling aspect, computation is also a critical issue of segmentation in real applications. Many variational segmentation models use level set formulation [25] to deal with the problem of topology changes during contour evolution, and have showed promising results. However, the computational cost of level set based approaches can be high in the commonly used semi-implicit implementation. Also, it has been demonstrated that the method is sensitive to initial condition [9]. In addition, practical implementation of level set based segmentation usually requires techniques such as reinitialization or enforcing certain penalty terms to keep the level set function from being too flat [22], [26]. As an alternative, we directly work on the characteristic functions of the partition regions. Then the regularization term that penalizes lengths of partition curves is equal to the total variations (TV) of the characteristic functions, and the new objective function is convex with respect to these functions. However, the minimization is still difficult to carry out due to the non-convexity of the solution set, which is later shown to be the tensor product of vertices of a canonical simplex. For multiphase segmentation, we relax the constraint to the entire simplex before solving the minimization problem. Then we truncate the final result and obtain a characteristic function as our segmentation result. This is an extension of the idea proposed in [27], [28] for two-phase segmentation. In that case, there is a single characteristic function with binary constraint appeared in the minimization. After relaxation, the constraint becomes the unit interval and hence can be handled relatively easily, see, e.g. [27], [29]. Moreover, theoretical results on the equivalence between the original and relaxed problems can be established. However, the situation becomes much more complicated when the problem levels up to multiphase segmentation, mainly due to the simplex constraints and multiple non-smooth TV terms involved in optimization. In this paper, we propose an effective numerical algorithm that utilizes the primal-dual formulation of TV norms and

special properties of canonical simplex to quickly approximate a solution. The primal-dual formulation has been successfully applied to TV based image reconstruction to achieve very promising efficiency [30], [31]. In this paper, we utilize the similar idea to derive a fast segmentation algorithm which involves only convolutions using kernel function with small support, and pointwise projections onto the unit ball and canonical simplex. To demonstrate the effectiveness of our method, we test the proposed algorithm on various images, and make comparisons with the state-of-the-art algorithms.

The rest of this paper is organized as follows. In the next section, we derive the model for joint image segmentation and bias field estimation. In Section III, we develop a fast numerical algorithm via the primal-dual gradient projections. Section IV presents the results on a number of images and evaluates the performance of the proposed algorithm with comparisons to several recently proposed methods in the field. The last section concludes the paper.

## II. MODEL FORMULATION

### A. Multiphase Segmentation and MAP Approach

We first establish a generalized multiphase image segmentation framework for joint region partitioning and intensity bias correction. Suppose  $I : \Omega \rightarrow \mathbb{R}$  is the input image to be segmented, where  $\Omega \subset \mathbb{R}^d$  is a closed and bounded region that represents the domain of  $I$ , and  $d$  is the dimension of the image (usually 2 or 3). For ease of presentation, we only consider rectangular gray-valued images in this paper. Given image  $I$ , the purpose of image segmentation is to partition its domain  $\Omega$  into several (say  $M$ ) regions, such that each region delineates an image pattern distinct from those by other regions. Namely, we need to solve for a set of regions  $\{\Omega_i\}_{i=1}^M$  such that  $\Omega = \cup_{i=1}^M \Omega_i$ ,  $\{\Omega_i\}_{i=1}^M$  are disjoint, and  $\Omega_i$  indicates the support of the  $i$ -th pattern in image  $I$ . This is equivalent to solving for the collection of characteristic functions  $\chi_i(x)$  of  $\Omega_i$ , where

$$\chi_i(x) = \begin{cases} 1 & \text{if } x \in \Omega_i, \\ 0 & \text{otherwise,} \end{cases} \quad (1)$$

for  $i = 1, \dots, M$ , and  $\sum_i \chi_i(x) = 1, \forall x \in \Omega$ .

As addressed in the introduction section, the input image  $I$  can be corrupted by noise and unknown intensity bias field  $b: \Omega \rightarrow \mathbb{R}$ . That is

$$I(x) = b(x)I_0(x) + n(x) \quad (2)$$

where  $I_0$  is the ideal clean image. Consider the simple case where the ideal image is constant  $c_i$  in each region  $\Omega_i$ , and the noise  $n(x)$  is normally distributed and independent of those at other locations. More precisely, if  $x \in \Omega_i$ , then

$$I(x) = b(x)c_i + n_i(x) \quad (3)$$

where  $n_i(x)$  is normally distributed with mean zero and unknown variance  $\sigma_i^2$ . It is worth noting that different applications may yield changes in the modeling of (3) [12]. Nevertheless, the derivation and resulting algorithms given below still work with appropriate modifications accordingly.

To this end, we can see that a complete solution package to an image segmentation with bias field estimation problem

is  $\{\chi, b, c, \sigma\}$ , where  $\chi = (\chi_1, \dots, \chi_M)^T: \Omega \rightarrow \{0, 1\}^M$ ,  $c = (c_1, \dots, c_M)^T \in \mathbb{R}^M$  and  $\sigma = (\sigma_1, \dots, \sigma_M)^T \in \mathbb{R}_+^M$ . Here  $\chi_i$ , the  $i$ -th component of  $\chi$ , is the characteristic function of  $\Omega_i$  as defined in (1),  $c_i$  and  $\sigma_i^2$  represent the original mean intensity and noise variance in region  $\Omega_i$ .  $b$  is unknown bias field that causes intensity inhomogeneity in the image.

We first find the posterior probability distribution  $p(\{\chi, b, c, \sigma\}|I)$  of  $\{\chi, b, c, \sigma\}$  given image  $I$ , and then obtain an optimal segmentation and bias field estimation by the maximum-a-posteriori (MAP). Note that the Bayes' rule implies that

$$p(\{\chi, b, c, \sigma\}|I) \propto p(I|\{\chi, b, c, \sigma\})p(\{\chi, b, c, \sigma\}). \quad (4)$$

Therefore, we need to determine  $p(\{\chi, b, c, \sigma\})$ , the prior information imposed to  $\{\chi, b, c, \sigma\}$ , and  $p(I|\{\chi, b, c, \sigma\})$ , the joint distribution of pixel intensities given  $\{\chi, b, c, \sigma\}$ .

### B. Modeling the Intensity Inhomogeneity

Based on model (3), one can see that  $I(x)$  is normally distributed as  $\mathcal{N}(b(x)c_i, \sigma_i^2)$  if  $x \in \Omega_i$  (or  $\chi_i(x) = 1$ ) given the segmentation  $\{\chi, b, c, \sigma\}$ . However, the observed intensity  $I(x)$  is merely one realization and it is usually not reliable to recover  $\chi, b, c$  and  $\sigma$  simultaneously. For robust density function estimation, we use the intensity density functions of neighbor pixels in  $W_x$  to approximate  $p(I(x)|\{\chi, b, c, \sigma\})$  in MAP (4). More precisely, we model  $p(I(x)|\{\chi, b, c, \sigma\})$  using a multiplicative density structure of  $I(x)$  as follows,

$$p(I(x)|\{\chi, b, c, \sigma\}) \propto \prod_{y \in W_x^\rho} (p(I(y)|\{\chi, b, c, \sigma\}))^{\pi_x(y)}, \quad (5)$$

where  $W_x^\rho = \{y \in \Omega : |y - x| \leq \rho\}$  is a circular image neighborhood with prescribed radius  $\rho$  and centered at  $x$ . On the right hand side of (5), we consider that  $I(y)$  closely follows the model (3) and contributes to the density function of  $I(x)$  via a weighted product as in (5). In (5),  $\pi_x: W_x^\rho \rightarrow [0, 1]$  gives the weights of intensity distributions of the points in  $W_x^\rho$  such that  $\sum_{y \in W_x^\rho} \pi_x(y) = 1$ . One can simply choose  $\pi_x(y) = 1/|W_x^\rho|$  for all  $y \in W_x^\rho$  if the intensities of neighbor points in  $W_x^\rho$  make equal contributions to the probability distribution  $p(I(x)|\{\chi, b, c, \sigma\})$ . In this paper, alternatively, we use more adaptive weights  $\pi_x(y)$  according to the distance from  $y$  to the center  $x$  via

$$\pi_x(y) = \mathcal{K}_s(y - x), \quad (6)$$

where  $\mathcal{K}_s$  a (truncated) Gaussian kernel function defined by

$$\mathcal{K}_s(z) = \begin{cases} C \exp(-|z|^2/2s^2), & \text{if } |z| \leq \rho \\ 0 & \text{otherwise.} \end{cases} \quad (7)$$

for some  $s > 0$ . In (7),  $C$  is a normalizing constant that makes  $\int_{|z| \leq \rho} \mathcal{K}_s(z) dz = 1$ .

We observe that the intensity bias field in practical applications usually varies gradually across the image domain. In another words, the value  $b(y)$  is nearly constant for points  $y$  in an image patch  $W_x^\rho$  provided that  $\rho$  is not too large. Therefore, we approximate  $b(y)$  by  $b(x)$ , the bias at the center point  $x$ ,

and obtain that  $I(y) \sim \mathcal{N}(b(x)c_i, \sigma_i^2)$  for  $y \in W_x^\rho \cap \Omega_i$ . Hence, the joint distribution  $p(I|\{\chi, b, c, \sigma\})$  in (5) can be obtained:

$$p(I|\{\chi, b, c, \sigma\}) = \prod_{x \in \Omega} \prod_{y \in W_x^\rho} p(I(y)|\{\chi, b, c, \sigma\})^{\mathcal{K}_s(y-x)} \quad (8)$$

where  $p(I(y)|\{\chi, b, c, \sigma\})$  is Gaussian-type

$$\frac{1}{\sqrt{2\pi\sigma_i^2}} \exp\left(-\frac{|I(y) - b(x)c_i|^2}{2\sigma_i^2}\right) \quad (9)$$

for those points  $y$  that  $\chi_i(y) = 1$ . By now, we have established the conditional probability density  $p(I|\{\chi, b, c, \sigma\})$  in (4).

On the other hand, we set the prior of  $\chi$  according to the descriptive length of the boundaries  $\partial\Omega_i$  to exponential distribution with parameter  $\alpha$ , which implicitly penalizes undesired irregular and zigzag partition curves. The priors of  $b, c$  and  $\sigma$  are imposed non-informatively. In addition, terms in  $\{\chi, b, c, \sigma\}$  are assumed to be independent. Consequently, the prior  $p(\{\chi, b, c, \sigma\})$  can be simplified to

$$p(\{\chi, b, c, \sigma\}) \propto \prod_{i=1}^M \exp(-\alpha|\partial\Omega_i|). \quad (10)$$

Based on (8) and (10), the MAP of (4) is equivalent to the following minimization after we applied negative logarithm to both sides of (4),

$$\min_{\chi, b, c, \sigma} \left\{ \alpha \sum_{i=1}^M |\partial\Omega_i| + L(\{\chi, b, c, \sigma\}) \right\}. \quad (11)$$

Here  $L(\{\chi, b, c, \sigma\})$  is the negative log-likelihood function

$$\begin{aligned} L(\{\chi, b, c, \sigma\}) &= -\log p(I|\{\chi, b, c, \sigma\}) \\ &= \int_{\Omega} \sum_{i=1}^M \int_{W_x^\rho \cap \Omega_i} \mathcal{K}_s(y-x) l_i(y; x) dy dx \\ &= \int_{\Omega} \sum_{i=1}^M \int_{\Omega} \chi_i(y) \mathcal{K}_s(y-x) l_i(y; x) dy dx \end{aligned} \quad (12)$$

and  $l_i(y; x)$  is defined for  $y \in \Omega_i \cap W_x^\rho$  by

$$l_i(y; x) := \frac{|I(y) - b(x)c_i|^2}{2\sigma_i^2} + \frac{1}{2} \log(2\pi\sigma_i^2). \quad (13)$$

In (12), we substituted the summation by integral to accommodate the continuous setting of our derivation, and omitted  $W_x^\rho$  and  $\Omega_i$  in the last equality according to the definitions of  $\mathcal{K}_s$  and  $\chi_i$  in (7) and (1), respectively. We point out here that the data fitting structure (12) using Gaussian distribution (9) with constant variance has been used in previous work [20], [21], [24] for image segmentation in the presence of intensity inhomogeneity. The derivation above provides a MAP point of view of this approach. Varying assumptions on intensity or noise distribution, one can also modify (3) and (9) accordingly and obtain an adaptive term (12) to solve specific image segmentation problems.

To write the first term in (11) using the characteristic functions  $\chi_i$ , we recall that the total variation of a function  $f : \Omega \rightarrow \mathbb{R}$  is defined by

$$TV(f) = \sup_{p \in Y} \left\{ - \int_{\Omega} f \operatorname{div} p dx \right\} \quad (14)$$

where the admissible set  $Y$  is

$$Y := \{p \in C_0^\infty(\Omega; \mathbb{R}^d) : |p(x)| \leq 1, \forall x \in \Omega\}. \quad (15)$$

Since  $\chi_i$  is the characteristic function of  $\Omega_i$ , the total variation of  $\chi_i$  is then the descriptive length of  $\partial\Omega_i$  by coarea formula:

$$TV(\chi_i) = |\partial\Omega_i|. \quad (16)$$

Plug (16) and (12) into (11), we obtain a generalized multiphase segmentation model as follows,

$$\min_{\chi, b, c, \sigma} \sum_{i=1}^M \left\{ \alpha TV(\chi_i) + \int_{\Omega} \chi_i(x) h_i(x) dx \right\} \quad (17)$$

subject to the constraint that only one component in  $\chi(x) = (\chi_1(x), \dots, \chi_M(x))^T$  is 1 and the others are 0 at each  $x \in \Omega$ . In (17), the function  $h_i$  is defined by

$$h_i(x) = \int_{\Omega} \mathcal{K}_s(y-x) l_i(x; y) dy. \quad (18)$$

The second term in (17) is obtained by exchanging the symbols  $x$  and  $y$ , followed by switching the order of integrations.

### III. NUMERICAL ALGORITHM

Although the segmentation problem has been unified to (17), this minimization problem cannot be solved efficiently in general due to the non-differentiability of the TV term, and the nonconvexity of the objective function with respect to  $\{\chi, b, c, \sigma\}$ . Conventional approaches based on level set formulation require extensive computations and suffer the local minimums severely. In this paper, we develop an efficient numerical algorithm to tackle the computation of (17).

We first relax the constraint on the characteristic function  $\chi = (\chi_1, \dots, \chi_M)^T$  in (17) to  $X$  defined by

$$X := \{u : \Omega \rightarrow [0, 1]^M \mid u(x) \in \Delta^M, \forall x \in \Omega\} \quad (19)$$

and the canonical simplex  $\Delta^M$  is defined by

$$\Delta^M = \{(z_1, \dots, z_M)^T \in \mathbb{R}_{\geq 0}^M : z_1 + \dots + z_M = 1\} \quad (20)$$

The relaxed model of (17), using notation  $u$  instead of conventional binary function  $\chi$ , becomes

$$\min_{u, b, c, \sigma} \sum_{i=1}^M \left\{ \alpha TV(u_i) + \int_{\Omega} u_i(x) h_i(x) dx \right\} \quad (21)$$

subject to  $u \in X$ . One can readily see that the original constraint in (17) further requires  $u(x)$  to be one of the vertices of  $\Delta^M$ . This relaxation substitutes the solution set of  $u$  by a continuous and convex set.

In the rest part of this section, we use alternating minimizations to construct an iterative algorithm. Namely, we need to minimize the objective function with respect to one of the variables in  $\{u, b, c, \sigma\}$  with others fixed at a time.

#### A. First Variations of $b$ , $c$ , and $\sigma$

First of all, we observe that the variables  $b$ ,  $c$ , and  $\sigma$  only appear in the second term of the objective function in (21), and their solutions can be obtained by first variations.

Fix  $u$ ,  $c$  and  $\sigma$ , we compute the Euler-Lagrangian (E-L) equation for  $b$  and obtain

$$b(x) = \frac{\sum_{i=1}^M (c_i/\sigma_i^2) [\mathcal{K}_s * (u_i I)](x)}{\sum_{i=1}^M (c_i^2/\sigma_i^2) [\mathcal{K}_s * u_i](x)}, \quad x \in \Omega, \quad (22)$$

where  $*$  is the convolution operator. Next, we fix  $u$ ,  $b$ , and  $\sigma_i$  and obtain the E-L equation of  $c_i$  for each  $i = 1, \dots, M$  as

$$c_i = \frac{\int_{\Omega} [\mathcal{K}_s * (u_i b I)](x) dx}{\int_{\Omega} [\mathcal{K}_s * (u_i b^2)](x) dx}. \quad (23)$$

Finally we have the E-L equation of  $\sigma_i$  as

$$\sigma_i^2 = \frac{\int_{\Omega} ([\mathcal{K}_s * (u_i I^2)] - 2c_i b [\mathcal{K}_s * I] + c_i b^2) dx}{\int_{\Omega} [\mathcal{K}_s * u_i] dx}. \quad (24)$$

Therefore, the updates of  $b$ ,  $c$  and  $\sigma$  have closed forms and the main computations are regular convolutions using kernel function  $\mathcal{K}_s$  defined in (7).

#### B. Solution to $u$

Now we turn to the minimization of the objective function (21) with respect to  $u$ . For fixed  $b$ ,  $c$  and  $\sigma$ , the minimization can be written as

$$\min_{u \in X} \sum_{i=1}^M \left\{ \alpha TV(u_i) + \int_{\Omega} u_i(x) h_i(x) dx \right\}, \quad (25)$$

where  $h_i$  does not depend on  $u$  according to its definition in (18). We remark that (25) is a constrained nonsmooth optimization problem due to the constraint on  $u(x) \in \Delta^M$  for each  $x \in \Omega$  and the nondifferentiable TV term. So we need to find an effective way to tackle these two issues.

For each  $u_i$ , we introduce the dual variable  $p_i \in Y$  according to the definition in (14), and rewrite the minimization problem (25) as a min-max problem

$$\min_{u \in X} \max_{p_i \in Y} \sum_{i=1}^M \left\{ -\alpha \int_{\Omega} u_i \operatorname{div} p_i dx + \int_{\Omega} u_i h_i dx \right\}, \quad (26)$$

where  $X$  is defined in (19) and  $Y$  is the admissible set of  $p_i$ 's defined in (15). The objective function in (26) is convex with respect to primal variable  $u$  and concave to dual variable  $p$ . The sets  $X$  and  $Y$  are both closed and convex. Therefore classical theory of saddle points of min-max problem applies [32]. Moreover, a fast primal-dual hybrid gradient scheme was introduced by Zhu and Chan in [30] and then extensively used for imaging applications, especially for TV based image reconstruction problems. In this paper, we adopt such a primal-dual update scheme, and introduce fast projections so that the computations in such scheme can be carried out efficiently.

In the discrete setting where the image  $I$  consists of  $N$  pixels, we can vectorize each  $u_i$  into a column vector in  $\mathbb{R}^N$ , then its dual variable  $p_i$  is a matrix in  $\mathbb{R}^{N \times d}$ , where  $d$  is the

dimension of the image (e.g. 2 or 3). Hence, the optimization problem (26) can be written as

$$\min_{u \in X} \max_{p_i \in Y} F(u, p) := \sum_{i=1}^M \langle u_i, \alpha D^T p_i + h_i \rangle, \quad (27)$$

where  $D : \mathbb{R}^N \rightarrow \mathbb{R}^{N \times d}$  is the discretized gradient operator, the superscript  $T$  is the conjugate operator, and  $\langle \cdot, \cdot \rangle$  represents the regular inner product in  $\mathbb{R}^N$ .

Note that both of  $X$  and  $Y$  are closed and convex sets. Hence a solution to the min-max problem (27) can be obtained by alternately solving for the primal variable  $u$  and dual variable  $p$

$$u^{k+1} = \Pi_X([u_i^k - \delta_k(\alpha D^T p_i^{k+1} + h_i)]_{i=1}^M), \quad (28)$$

$$p_i^{k+1} = \Pi_Y(p_i^k + \tau_k D u_i^k), i = 1, \dots, M. \quad (29)$$

where  $\delta_k$  and  $\tau_k$  act as the step sizes of the primal and dual variables  $u$  and  $p$  in the  $k$ -th iteration, respectively, and  $[u_i]_{i=1}^M$  denotes the matrix  $[u_1, \dots, u_M]$  that has  $u_i$  as columns. Here  $\Pi_X : \mathbb{R}^{N \times M} \rightarrow X$  and  $\Pi_Y : \mathbb{R}^{N \times d} \rightarrow Y$  are projection operators onto the sets  $X$  and  $Y$ , respectively. More precisely,  $\Pi_X$  maps each row of its argument, say  $z \in \mathbb{R}^M$ , to the simplex  $\Delta^M$  using the algorithm shown in [33], [34], and  $\Pi_Y$  projects each row of its argument, say  $z \in \mathbb{R}^d$ , to the unit ball  $B^d := \{z \in \mathbb{R}^d : \|z\|_2 = 1\}$  via

$$z \mapsto \frac{z}{\max\{\|z\|_2, 1\}}. \quad (30)$$

We note that the projections  $\Pi_X$  and  $\Pi_Y$  mentioned above have complexity  $M \log M$  and  $Md$ , respectively. Therefore, the main computational cost is  $NM(\log M + d)$  in each iteration. Note that  $M$  is the number of phases in the image and is usually less than 10, and  $d$  is the dimension of the image such as 2 or 3. Moreover, these projections are applied to each of the  $N$  pixels and hence the computations in both of  $\Pi_X$  and  $\Pi_Y$  can be carried out in parallel. On the contrary, level set function based segmentation with commonly used semi-implicit gradient descent scheme usually requires Gauss eliminations to solve tridiagonal linear systems, and hence the computation cannot be parallelized easily.

### C. Algorithm

In conventional settings of alternating minimizations, we need to iterate (28) and (29) until convergence to get  $u$  before updating the other variables  $b$ ,  $c_i$  and  $\sigma_i$ ,  $i = 1, \dots, M$ . However, we found that empirically it is more efficient to simply solve for  $u$  and  $p$  only once and immediately update the remaining variables.

The stopping criterion of the proposed algorithm is set to  $\|u^k - u^{k-1}\|_2 / \|u^k\|_2 < \epsilon_{\text{tol}}$ . Namely, the computation is automatically terminated if the relative change in the iterate  $\{u^k\}$  is less than a prescribed tolerance value  $\epsilon_{\text{tol}}$ .

As we have relaxed the constraint on the function  $u$ , the resulting  $u$  may contain values in  $(0, 1)$  and hence are not characteristic functions. Therefore, once  $u$  is obtained, we further threshold the components of  $u(x)$  to  $\bar{u}(x)$  by

$$\bar{u}_i(x) = \begin{cases} 1 & \text{if } u_i(x) = \max_{1 \leq j \leq M} \{u_j(x)\} \\ 0 & \text{otherwise} \end{cases} \quad (31)$$

---

### Algorithm 1 Fast Multiphase Segmentation (FastSEG)

---

Input  $\alpha > 0$  and  $\epsilon_{\text{tol}}$ . Initialize  $u^0$  and  $p^0$ , and set  $b^0 = 1$ ,  $k = 0$ .

**repeat**

Update  $c^k$  using (23) with  $u^k$  and  $b^k$ ;  
 Update  $\sigma^k$  using (24) with  $u^k$ ,  $b^k$  and  $c^k$ ;  
 Compute  $h^k$  using (18) with  $b^k$ ,  $c^k$  and  $\sigma^k$ ;  
 Compute  $u^k$  using (28) with  $h^k$ ;  
 Compute  $p^k$  using (29) with  $h^k$ ;  
 Update  $b^k$  using (22) with  $u^k$ ,  $c^k$  and  $\sigma^k$ ;  
 $k \leftarrow k + 1$ .

**until**  $\|u^k - u^{k-1}\|_2 / \|u^k\|_2 < \epsilon_{\text{tol}}$

Compute  $\bar{u}$  using (31) and return  $\{\bar{u}, b, c, \sigma\}$ .

---

for each  $x \in \Omega$ . If there are several equally maximal values in  $u(x)$ , we just pick one randomly.

To sum up, we propose a fast segmentation (FastSEG) algorithm in Algorithm 1 below.

## IV. EXPERIMENTAL RESULTS

In this section, we test the Algorithm 1 on a variety of images and compare with recently proposed methods for image segmentation in the presence of noise and intensity bias.

### A. Experiment Settings

The proposed algorithm is implemented and all the tests are performed in MATLAB®7.9 (R2009b) computing environment on a PC with Intel Dual Core 2 Duo CPU at 2.4 GHz (only one core is used in computation) and 3 GB of memory. We expect a significant improvement in computation speed if the program is parallelized.

In this paper, we always determine the number of phases  $M$  for an input image. We use initialization in the same way as that of the comparison algorithms if available. In particular, as our algorithm does not employ level set functions, we set  $u^0$  in Algorithm 1 to the characteristic functions of the regions delineated by the initial contours in the comparison algorithms. For other experiments, we use  $K$ -means algorithm to the collection of pixel intensities of the given image, and assign  $u_i^0(x) = 1$  if the  $K$ -means algorithm classifies  $x$  to the  $i$ -th group and 0 otherwise for  $i = 1, \dots, M$ . Note that the minimizations in segmentation problems are nonconvex in general, and hence it is usually preferred to start from an initial guess close to the desired partition. The  $K$ -means algorithm can generate close approximations to the desired segmentation if there are slight noise and intensity bias. However, we can observe unsatisfactory initialization by  $K$ -means for many images tested in this paper. For instance, Figure 4(a) shows the initial guess obtained by  $K$ -means, which is not quite close to the final optimal segmentation shown in Figure 4(f). Nevertheless, the proposed algorithm is still shown to be very robust with respect to different initializations in Section IV-C.1.

We use test images and default parameter settings in the original code of comparison algorithms if available. For the proposed algorithm, the stopping criterion  $\epsilon_{\text{tol}}$  is set to  $10^{-3}$  throughout the experiments. The parameters  $\alpha$ ,  $\delta_k$  and  $\tau_k$  are

set to be  $10^{-4}$ , 0.2 and 0.5 respectively. The patch radius  $\rho$  is set to 8, and the variance  $s$  is 4 in (7). For all images we tested (whose intensities are scaled to  $[0,1]$ ), they seem to provide good compromise between smoothness and accuracy as well as speed and stableness. We also found that moderate changes in these parameters do not yield significant difference in segmentation results.

### B. Quantitative Evaluation and Comparison With Existing Methods

We use Jaccard similarity coefficient as a quantitative measure to evaluate the segmentation results. Let  $\Omega_i$  be the  $i$ -th region obtained by the algorithm and  $\bar{\Omega}_i$  be its corresponding region in the ground truth image, then the JSC between  $\Omega_i$  and  $\bar{\Omega}_i$  is defined as

$$J(\Omega_i, \bar{\Omega}_i) = \frac{|\Omega_i \cap \bar{\Omega}_i|}{|\Omega_i \cup \bar{\Omega}_i|}, \quad (32)$$

where  $|\cdot|$  represents the area of a region. Generally speaking, Jaccard similarity coefficients is bounded in  $[0, 1]$  and larger values imply more accurate segmentation.

To demonstrate the effectiveness of the proposed model, we compare it with three recently developed methods in this field. For completeness, we give a brief summary regarding these methods in the following.

1) *Comparison Methods*: To demonstrate the efficiency of the proposed algorithm, we make comparisons to three mostly related segmentation methods with intensity bias field estimation.

The first method we are going to compare is the Weighted  $K$ -means Variational Level Set (WKVLS) method [22]. For the two-phase case, the WKVLS model can be written as

$$\begin{aligned} E_W(\phi, b, c_1, c_2) &= \nu \int_{\Omega} |\nabla H(\phi)| dx + \mu \int_{\Omega} (|\nabla \phi| - 1)^2 dx \\ &+ \int_{\Omega} \int_{\Omega} H(\phi) \mathcal{K}_s(y-x) |I(y) - b(x)c_1|^2 dy dx \\ &+ \int_{\Omega} \int_{\Omega} (1 - H(\phi)) \mathcal{K}_s(y-x) |I(y) - b(x)c_2|^2 dy dx, \end{aligned} \quad (33)$$

where  $\phi$  is the level set function whose zero level set represents the partition contour, and  $H$  is the Heaviside function defined by  $H(z) = 1$  if  $z \geq 0$  and 0 otherwise. The first two terms in (33) penalize the length of partition contour and force the level set function  $\phi$  to be up straight (has slope 1) during evolutions. The last two terms in (33) are for data fitting as in the proposed algorithm, but lack the variability of noise level  $\sigma_i$ .

The next one is the Statistical and Variational Multiphase Level Set (SVMLS) method [24], which also utilizes level set formulation and minimizes the following energy functional

$$E_S(\Phi, b, c, \sigma) = \sum_{i=1}^4 \int_{\Omega} \int_{\Omega} M_i(\Phi(y)) \mathcal{K}_s(y-x) l_i(y; x) dy dx, \quad (34)$$

where  $l_i(y; x)$  is the same as that in (13),  $\Phi = (\phi_1, \phi_2)$ , and  $M_i(\Phi)$  is defined as follows:

$$\begin{cases} M_1(\Phi) = H(\phi_1)H(\phi_2), \\ M_2(\Phi) = H(\phi_1)(1 - H(\phi_2)), \\ M_3(\Phi) = (1 - H(\phi_1))H(\phi_2), \\ M_4(\Phi) = (1 - H(\phi_1))(1 - H(\phi_2)). \end{cases} \quad (35)$$

The last method we would compare is the Coherent Local Intensity Clustering (CLIC) method [20]. CLIC partitions an image by solving a constrained minimization problem,

$$\begin{aligned} E_C(b, u, c) &= \sum_{i=1}^M \int_{\Omega} \int_{\Omega} u_i(y) \mathcal{K}_s(y-x) |I(y) \\ &\quad - b(x)c_i|^2 dy dx, \\ \text{subject to} &\quad \sum_{i=1}^M u_i(x) = 1, \quad \forall x \in \Omega. \end{aligned} \quad (36)$$

In the first comparison experiment below, we used the default test image and parameter setting for SVMLS using the online source code package, and manually tuned the parameters of WKVLS, CLIC, and the proposed method until the best visual quality was achieved for each method. We also extensively tested reasonable parameters settings of all comparison methods for the BrainWeb data in the second experiment, and presented the result of each method that reached the highest average JSC score respectively.

2) *Experiment I*: In the first experiment, we compare the proposed model with the aforementioned three methods on an MR brain image with strong intensity inhomogeneity and noise. We use the default test image (shown in Figure 2(a)) from the source code package of SVMLS published online<sup>1</sup>. The initial conditions (shown in Figure 2(b)) is also the default setting for the SVMLS code and is used for all the tested algorithms. For this experiment, we only provide visual results in Figure 2 since a ground truth segmentation is not available.

The input image shown in Figure 2(a) contains strong intensity inhomogeneity and hence it is difficult to distinguish different tissue intensities from its histogram as shown in Figure 2(c). Therefore, conventional approaches based on intensity clustering do not return correct partitions. On the other hand, all the four tested algorithms can generate reasonable results by taking the intensity inhomogeneity into account.

It can be seen that the corrected images have less intensity biases compared to 2(a). This can also be observed in their histograms shown in the second row of Figure 2. The histograms of the corrected images have clear intensity peaks and hence different tissues can be distinguished more easily.

As the intensity bias field  $b$  is also estimated by these algorithms, we plot  $I/b$ , the images after bias correction, in the second row of Figure 2. Here  $/$  represents pointwise division. We note here that the model has an ambiguity with regards to  $b(x)$  and the  $\{c_i\}_i$  as shown in (3). So we normalized  $b(x)$  obtained from different methods into  $[0, 1]$  before displaying  $I/b$ . In this case, the images have comparable grey scales.

When we look into the details of the segmentation results, we can observe that those obtained by CLIC and the proposed

<sup>1</sup><http://www4.comp.polyu.edu.hk/~cslzhang/code.htm>

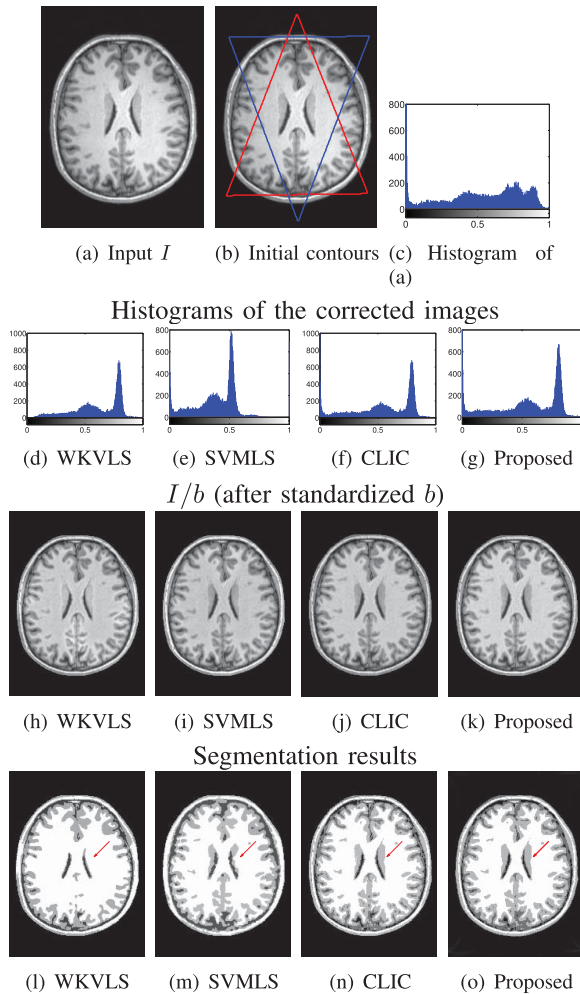


Fig. 2. Comparison of the proposed model with WKVLS, SVMLS and CLIC on an MR brain image (a) with strong intensity inhomogeneity. The color squares in (a) depict initial contours used by all methods.

algorithm are more accurate than those by WKVLS and SVMLS: the former two can better separate the gray and white matters as indicated by the red arrows in Figure 2(i)–2(o). One of the possible reasons is that WKVLS and SVMLS are formulated in that level set framework and hence can be easily trapped into local minimum.

3) *Experiment II*: The test image in this experiment is an MR image obtained from BrainWeb<sup>2</sup>. As ground truth segmentation is available in this case, we use Jaccard similarity coefficient to evaluate the performance of the test algorithms quantitatively.

In Figure 3, we use the same initialization for all the above mentioned segmentation models as shown by the red and blue rectangles in Figure 3(a). The ground truth obtained from BrainWeb are presented in Figure 3(b), which consists of four parts: background, white matter, gray matter and cerebrospinal fluid (CSF). The segmentation results obtained by the proposed algorithm, WKVLS, SVMLS and CLIC are shown in Figure 3(c)–3(f), respectively. The Jaccard similarity coefficients and CPU time are summarized in Table I. WKVLS and

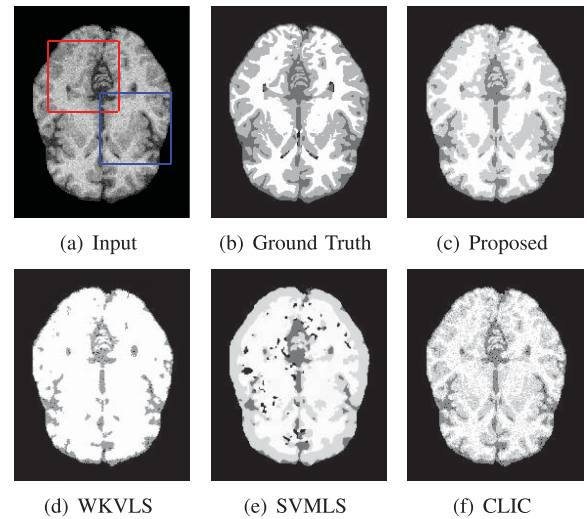


Fig. 3. Comparison of the proposed model, WKVLS, SVMLS and CLIC on an MR brain image with severe noise and intensity inhomogeneity.

TABLE I  
JACCARD SIMILARITY COEFFICIENTS  $JSC$  OF THE FOUR REGIONS, BACKGROUND (B), CSF (C), GREY MATTER (G) AND WHITE MATTER (W), OBTAINED BY THE TEST ALGORITHMS AND THEIR CPU TIME

Method	$JSC_b$	$JSC_c$	$JSC_g$	$JSC_w$	CPU (s)
WKVLS	48.87%	5.51%	25.63%	6.68%	160.82
SVMLS	69.71%	18.79%	42.84%	61.68%	21.90
CLIC	98.75%	70.76%	60.57%	65.96%	41.07
Proposed	99.13%	80.47%	80.69%	82.54%	33.75

SVMLS cannot return correct segmentation as evolution of the level set functions can be easily stuck at a local minimum. The result of CLIC are better than WKVLS and SVMLS, but it contains too many superfluous points due to the lack of proper regularization in such noisy case.

The proposed algorithm FastSEG exhibits promising efficiency compared to the other methods due to several reasons. First of all, FastSEG the directly solves for the characteristic functions whereas methods based on level set formulation need to propagate the front of level contour to reach desired partition. Secondly, the necessary regularization of partition curve using descriptive length is enforced accurately by TV of characteristic functions. Last but not least, the primal-dual gradient scheme can be adopted for the resulting min-max problem, and fast solvers such as simplex projection and kernel convolution can be implemented for low cost computations.

### C. Further Evaluations of the Proposed Algorithm

It is important that an automated segmentation procedure is robust with respect to different initial segmentations, intensity bias status, noise level, and parameter settings. In this subsection, we further evaluate the performance of Algorithm 1 on these aspects. Figures 4 to 7 followed by JSC Tables II to V correspondingly show the results.

1) *Robust to Initialization*: As the objective functions appeared in segmentation problems are usually nonconvex, most algorithms especially those formulated using level set functions, suffer local minimums and hence are very sensitive

<sup>2</sup><http://www.bic.mni.mcgill.ca/brainweb/>

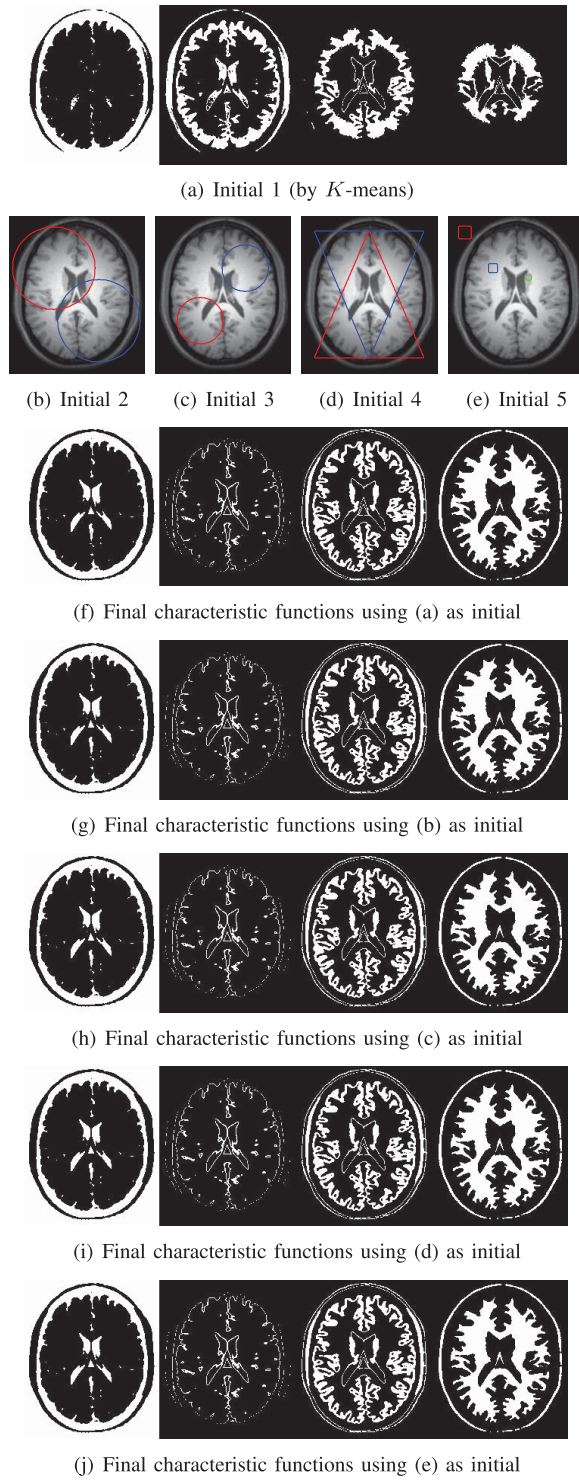


Fig. 4. Segmentation results of the proposed algorithm using different initializations.

to initializations. On the contrary, the proposed algorithm 1 appears to be robust: we test Algorithm 1 on an MR image using five different initializations as shown in Figures 4(a) (generated by *K*-means), 4(b), 4(c), 4(d), and 4(e) (generated by some seeds shown in red, green and blue squares). The final characteristic functions  $\chi_i$  obtained by the proposed algorithm are shown in Figures 4(f), 4(g), 4(h), 4(i) and 4(j), respectively. The results imply that the proposed algorithm is quite robust with respect different initial conditions.

TABLE II

JSC AND CPU TIME OF THE PROPOSED ALGORITHM USING DIFFERENT INITIALS AS SHOWN IN FIGURES 4(A) TO 4(E), RESPECTIVELY

Initial	$JSC_b$	$JSC_c$	$JSC_g$	$JSC_w$	CPU (s)
Init 1	99.98%	99.58%	99.83%	99.91%	14.63
Init 2	99.98%	99.46%	99.88%	99.97%	11.85
Init 3	99.99%	99.58%	99.90%	99.97%	12.18
Init 4	99.98%	99.46%	99.88%	99.96%	12.02
Init 5	99.83%	96.75%	99.00%	99.46%	13.75

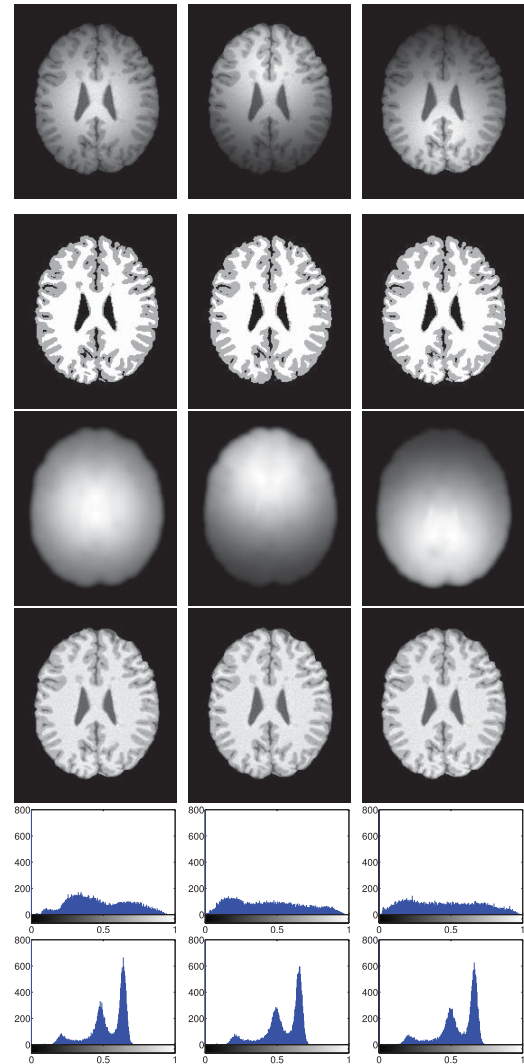


Fig. 5. Robustness test of the proposed algorithm on different intensity inhomogeneity. Left, middle, and right columns show segmentation results on images with intensity bias in the middle, top, and bottom of image domain, respectively. From top to bottom: input images, segmentation results, estimated bias fields, corrected images, histograms of input images, and histograms of corrected images, respectively.

2) *Robust to Intensity Inhomogeneity*: We conduct more experiments on Algorithm 1 on MR images to test its capability on different intensity inhomogeneities. The results are shown in Figure 5. The original MR images are obtained from BrainWeb. We add synthetic intensity biases to the image (concentrated at the middle, top and bottom of the image domain), as shown in the first row of Figure 5. We show the

TABLE III

JSC AND CPU TIME OF THE PROPOSED ALGORITHM ON DIFFERENT BIAS FIELDS SHOWN IN THE LEFT (L), MIDDLE (M), AND RIGHT (R) COLUMNS IN FIGURE 5

Column	$JSC_{bc}$	$JSC_g$	$JSC_{td}$	CPU (s)
L	98.96%	91.65%	94.76%	8.34
M	98.82%	86.86%	91.78%	20.40
R	99.48%	95.34%	95.87%	18.01

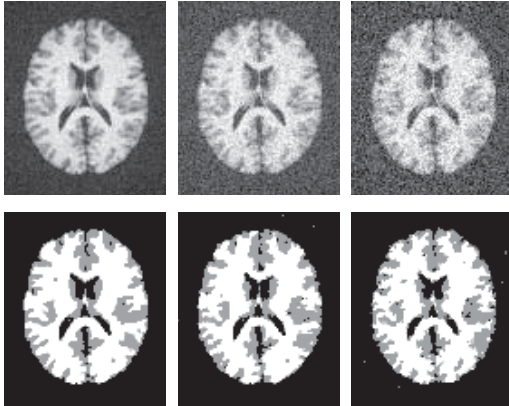


Fig. 6. Robustness test of the proposed algorithm on different image noise levels. Left, middle, and right columns correspond to small, medium and strong noise levels, respectively. Top and bottom rows show the input images and segmentation results, respectively.

TABLE IV

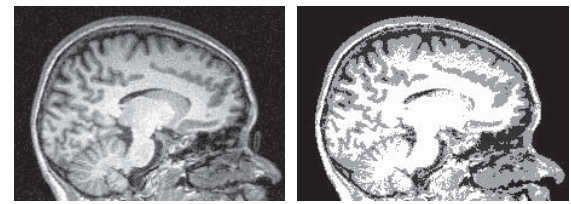
JSC AND CPU TIME OF THE PROPOSED ALGORITHM ON IMAGES WITH SMALL, MEDIUM, AND STRONG NOISES SHOWN IN FIGURE 6

Noise Level	$JSC_{bc}$	$JSC_g$	$JSC_{td}$	CPU (s)
Small	98.04%	76.47%	81.13%	2.68
Median	96.89%	74.53%	83.73%	3.08
Strong	95.75%	67.38%	78.37%	3.51

corrected images  $I/b$ , the recovered bias fields  $b$ , segmentation results, histograms of the test images and corrected images under each of these three images in Figure 5. We can see that Algorithm 1 successfully detects the intensity biases and obtains desired segmentations regardless of bias status.

3) *Robust to Noise Level*: The purpose of this experiment is to test Algorithm 1 on MR images with intensity inhomogeneity and different levels of noise. The test images are generated by first multiplying a simulated bias field to the clean MR image and then adding low, medium, and strong Gaussian noise. The segmentation results are presented in Figure 6. From the results shown in the second row of Figure 6, we can see that the proposed algorithm consistently returns reasonable partitions of the image, but the accuracy can be slightly affected by the noise level.

4) *Different Parameter Settings*: As shown in Section II, Algorithm 1 involves the penalty parameter  $\alpha$ , and step sizes  $\tau_k$  and  $\delta_k$  for the primal and dual variables. We found that the proposed algorithm performs well for a variety of images under the same setting of these parameters. However, the patch size  $\rho$  used for local density weight calculation in



(a) Input image

(b)  $\rho = 0$ (c)  $\rho = 2$ (d)  $\rho = 8$ 

K-mean initial (top) and segmentation result (bottom)

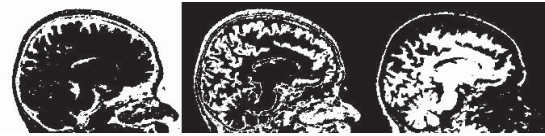
(e) Final characteristic function for  $\rho = 0$ (f) Final characteristic function for  $\rho = 2$ (g) Final characteristic function for  $\rho = 8$ 

Fig. 7. Efficiency of local intensity estimation in FastSEG when applied to images with strong noise.

TABLE V

JSC AND CPU TIME OF THE PROPOSED ALGORITHM WITH DIFFERENT PARAMETER  $\rho$  ON TEST IMAGE FIGURE 7(A)

$\rho$	$JSC_{bc}$	$JSC_g$	$JSC_{td}$	CPU (s)
0	89.06%	65.52%	82.07%	10.99
2	86.83%	67.14%	84.59%	12.30
8	89.61%	66.81%	86.15%	12.10

(7) can impact the results under different level of noise. In the following experiments we test Algorithm 1 with  $\rho = 0, \dots, 8$ . In particular, we show the results with  $\rho = 0, 2, 8$  in Figures 7(e)–7(g), respectively. Note that in Figure 7(e), there are many superfluous points in the case of  $\rho = 0$ , where local patch information is not utilized to estimate  $I(x)$ . On the other hand, the results look much better when we use the neighboring information. This suggests the importance of using local intensity density estimation (5), especially in the presence of strong noise.

## V. CONCLUSION

In this paper, we present a general multiphase soft segmentation framework which can deal with severe intensity inhomogeneity and noise. Our model estimates the intensity distribution at a particular pixel using a multiplicative structure of distributions of all pixels in a neighborhood, and derive the minimization problem using MAP. To tackle the computational difficulty due to the highly nonsmooth and constrained formulation of the segmentation model, we apply primal-dual gradient projections to develop a fast numerical algorithm. Numerical results on various images show that our method is more efficient and accurate in comparison with other recently proposed algorithms.

## REFERENCES

- [1] J. Canny, "A computational approach to edge detection," *IEEE Trans. Pattern Anal. Mach. Intell.*, vol. 8, no. 6, pp. 679–698, Nov. 1986.
- [2] V. Caselles, R. Kimmel, and G. Sapiro, "Geodesic active contours," *Int. J. Comput. Vision*, vol. 22, no. 1, pp. 161–179, 1997.
- [3] S. Kichenassamy, A. Kumar, P. Olver, A. Tannenbaum, and A. Yezzi, "Gradient flows and geometric active contour models," in *Proc. 5th Int. Conf. Comput. Vis.*, Jun. 1995, pp. 810–815.
- [4] R. Malladi, J. A. Sethian, and B. C. Vemuri, "Shape modeling with front propagation: A level set approach," *IEEE Trans. Pattern Anal. Mach. Intell.*, vol. 17, no. 2, pp. 158–175, Feb. 1995.
- [5] A. Vasilevskiy and K. Siddiqi, "Flux-maximizing geometric flows," *IEEE Trans. Pattern Anal. Mach. Intell.*, vol. 24, no. 12, pp. 1565–1578, Dec. 2002.
- [6] T. Chan and L. Vese, "Active contours without edges," *IEEE Trans. Image Process.*, vol. 10, no. 2, pp. 266–277, Feb. 2001.
- [7] R. Ronfard, "Region-based strategies for active contour models," *Int. J. Comput. Vis.*, vol. 13, no. 2, pp. 229–251, Oct. 1994.
- [8] C. Samson, L. Blanc-Feraud, G. Aubert, and J. Zerubia, "A variational model for image classification and restoration," *IEEE Trans. Pattern Anal. Mach. Intell.*, vol. 22, no. 5, pp. 460–472, May 2000.
- [9] L. Vese and T. Chan, "A multiphase level set framework for image segmentation using the Mumford and Shah model," *Int. J. Comput. Vis.*, vol. 50, no. 3, pp. 271–293, 2002.
- [10] D. Mumford and J. Shah, "Optimal approximations by piecewise smooth functions and associated variational problems," *Commun. Pure Appl. Math.*, vol. 42, no. 5, pp. 577–685, 1989.
- [11] S.-C. Zhu and A. Yuille, "Region competition: Unifying snakes, region growing, and Bayes/MDL for multiband image segmentation," *IEEE Trans. Pattern Anal. Mach. Intell.*, vol. 18, no. 9, pp. 884–900, Sep. 1996.
- [12] U. Vovk, F. Pernus, and B. Likar, "A review of methods for correction of intensity inhomogeneity in MRI," *IEEE Trans. Med. Imaging*, vol. 26, no. 3, pp. 405–421, Mar. 2007.
- [13] R. Guillemaud and M. Brady, "Estimating the bias field of MR images," *IEEE Trans. Med. Imaging*, vol. 16, no. 3, pp. 238–251, Jun. 1997.
- [14] J. Sled, A. Zijdenbos, and A. Evans, "A nonparametric method for automatic correction of intensity nonuniformity in MRI data," *IEEE Trans. Med. Imaging*, vol. 17, no. 1, pp. 87–97, Feb. 1998.
- [15] K. Van Leemput, F. Maes, D. Vandermeulen, and P. Suetens, "Automated model-based bias field correction of MR images of the brain," *IEEE Trans. Med. Imaging*, vol. 18, no. 10, pp. 885–896, Oct. 1999.
- [16] M. Styner, C. Brechbuhler, G. Szekely, and G. Gerig, "Parametric estimate of intensity inhomogeneities applied to MRI," *IEEE Trans. Med. Imaging*, vol. 19, no. 3, pp. 153–165, Mar. 2000.
- [17] J. Milles, Y. Zhu, G. Gimenez, C. Guttman, and I. Magnin, "MRI intensity nonuniformity correction using simultaneously spatial and gray-level histogram information," *Comput. Med. Imaging Graph.*, vol. 31, no. 2, pp. 81–90, 2007.
- [18] P. Vemuri, E. G. Kholmovski, D. L. Parker, and B. E. Chapman, "Coil sensitivity estimation for optimal SNR reconstruction and intensity inhomogeneity correction in phased array MR imaging," in *Proc. Inf. Process. Med. Imaging*, 2005, pp. 603–614.
- [19] C. Li, C. Gatenby, L. Wang, and J. Gore, "A robust parametric method for bias field estimation and segmentation of mr images," in *Proc. IEEE Conf. Comput. Vis. Pattern Recognit.*, Jun. 2009, pp. 218–223.
- [20] C. Li, C. Xu, A. W. Anderson, and J. C. Gore, "MRI tissue classification and bias field estimation based on coherent local intensity clustering: A unified energy minimization framework," *Inf. Process. Med. Imaging*, vol. 5636, pp. 288–299, Jul. 2009.
- [21] C. Li, R. Huang, Z. Ding, C. Gatenby, D. N. Metaxas, and J. C. Gore, "A level set method for image segmentation in the presence of intensity inhomogeneities with application to MRI," *IEEE Trans. Image Process.*, vol. 20, no. 7, pp. 2007–2016, Jul. 2011.
- [22] C. Li, R. Huang, Z. Ding, C. Gatenby, D. Metaxas, and J. Gore, "A variational level set approach to segmentation and bias correction of medical images with intensity inhomogeneity," in *Proc. 11th Int. Conf. Med. Image Comput. Comput. Assisted Intervent.*, 2008, pp. 1083–1091.
- [23] C. Li, C. Xu, C. Gui, and M. Fox, "Distance regularized level set evolution and its application to image segmentation," *IEEE Trans. Image Process.*, vol. 19, no. 12, pp. 3243–3254, Dec. 2010.
- [24] K. Zhang, L. Zhang, and S. Zhang, "A variational multiphase level set approach to simultaneous segmentation and bias correction," in *Proc. 17th IEEE Int. Conf. Image Process.*, Sep. 2010, pp. 4105–4108.
- [25] S. Osher and J. Sethian, "Fronts propagating with curvature-dependent speed: Algorithms based on Hamilton-Jacobi formulations," *J. Comput. Phys.*, vol. 79, no. 1, pp. 12–49, 1988.
- [26] K. Zhang, L. Zhang, H. Song, and D. Zhang, "Reinitialization-free level set evolution via reaction diffusion," *IEEE Trans. Image Process.*, vol. 22, no. 1, pp. 258–271, Jan. 2013.
- [27] X. Bresson, S. Esedoglu, P. Vanderghyest, J.-P. Thiran, and S. Osher, "Fast global minimization of the active contour/snake model," *J. Math. Imaging Vis.*, vol. 28, no. 2, pp. 151–167, Jun. 2007.
- [28] M. Nikolova, S. Esedoglu, and T. F. Chan, "Algorithms for finding global minimizers of image segmentation and denoising models," *SIAM J. Appl. Math.*, vol. 66, no. 5, pp. 1632–1648, 2006.
- [29] T. Goldstein, X. Bresson, and S. Osher, "Geometric applications of the split Bregman method: Segmentation and surface reconstruction," *J. Sci. Comput.*, vol. 45, nos. 1–3, pp. 272–293, 2010.
- [30] M. Zhu and T. Chan, "An efficient primal-dual hybrid gradient algorithm for total variation image restoration," Dept. Math., Univ. California, Los Angeles, Los Angeles, CA, USA, Tech. Rep. 08-34, 2008.
- [31] E. Esser, X. Zhang, and T. Chan, "A general framework for a class of first order primal-dual algorithms for tv minimization," *SIAM J. Imag. Sci.*, vol. 3, no. 4, pp. 1015–1046, 2010.
- [32] R. T. Rockafellar, *Convex Analysis*. Princeton, NJ, USA: Princeton Univ. Press, 1970.
- [33] Y. Chen and X. Ye, *Projection Onto A Simplex*. Berkeley, CA, USA: Univ. of California Press, Feb. 2011.
- [34] J. Duchi, S. S. Shwartz, Y. Singer, and T. Chandra, "Efficient projections onto the L1-ball for learning in high dimensions," in *Proc. 25th Int. Conf. Mach. Learn.*, pp. 272–279, 2008.



**Haili Zhang** is currently pursuing the Ph.D. degree with the Department of Mathematics with the University of Florida, Gainesville, FL, USA. She received the B.E. degree in mathematics from Henan Normal University, Xinxiang, China, and the M.S. degree in mathematics from Beijing Normal University, Beijing, China, in 2005 and 2008, respectively. Her current research interests include digital image processing, numerical analysis and partial differential equations.



**Xiaoqing Ye** is a Visiting Assistant Professor with the School of Mathematics, Georgia Institute of Technology, Atlanta, GA, USA. He received the Doctoral degree in mathematics from the University of Florida, Gainesville, FL, USA, in 2011. His current research interests include applied and computational mathematics, and their applications in image processing.



**Yunmei Chen** is a Full Professor of mathematics with the University of Florida, Gainesville, FL, USA. She received the Doctoral degree in mathematics from Fudan University, Shanghai, China, in 1985. Her current research interests include nonlinear partial differential equations, applied mathematics, mathematical modeling, computational methods, and their applications in image processing.